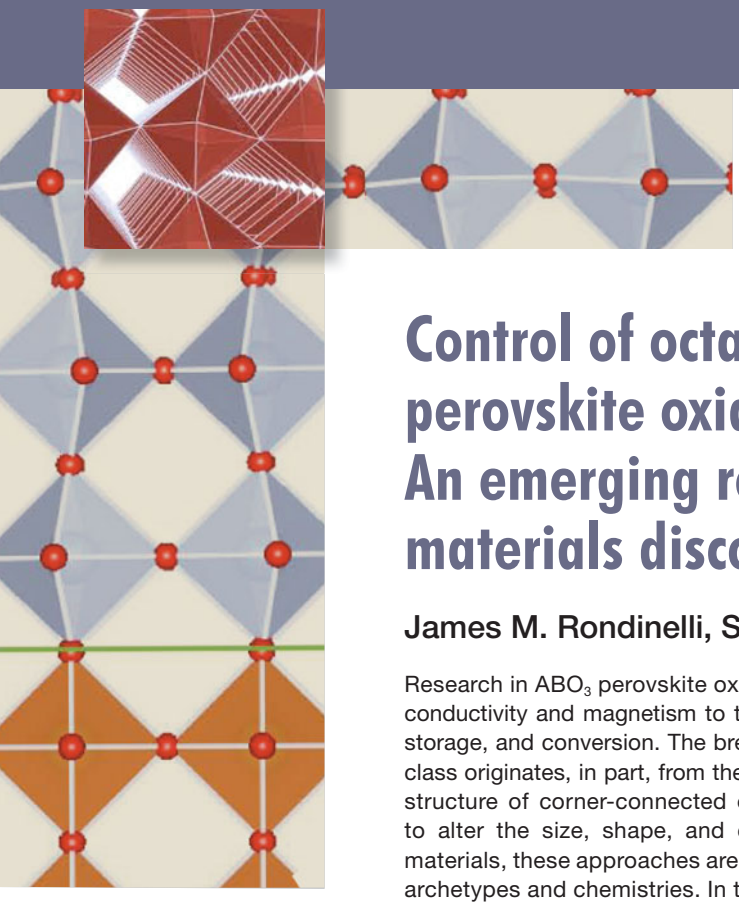

Control of octahedral connectivity in perovskite oxide heterostructures: An emerging route to multifunctional materials discovery

James M. Rondinelli, Steven J. May, and John W. Freeland

Research in ABO_3 perovskite oxides ranges from fundamental scientific studies in superconductivity and magnetism to technologies for advanced low-power electronics, energy storage, and conversion. The breadth in functionalities observed in this versatile materials class originates, in part, from the ability to control the local and extended crystallographic structure of corner-connected octahedral units. While an established paradigm exists to alter the size, shape, and connectivity of the octahedral building blocks in bulk materials, these approaches are often limited to certain subsets of the allowed perovskite archetypes and chemistries. In this article, we describe emerging routes in thin films and multilayer superlattices enabled by epitaxial synthesis aimed at engineering the octahedral connectivity—rotational magnitudes and patterns—to reach unexplored portions of the crystallographic structure–property phase space for rational materials design. We review three promising chemistry-independent strategies that provide a handle to tune the octahedral connectivity: epitaxial strain, interfacial control at perovskite/perovskite heterojunctions, and rotation engineering in short-period superlattices. Finally, we touch upon potential new functionalities that could be attained by extending these approaches to static and dynamic manipulation of the perovskite structure through external fields and highlight unresolved questions for the deterministic control of octahedral rotations in perovskite-structured materials.

Introduction

A common approach for designing functional materials involves the assembly of functional groups—a collection of atoms with unique properties that can be interwoven to create new materials. Organic chemists, for example, are able to tailor the reactivity, electronic structure, and mechanical properties of complex compounds through changes in the symmetry, arrangement, and coordination of such functional units on supporting "in-active" backbones.[1] Their inorganic colleagues, however, face substantial challenges: Those materials scientists who aim to rationally discover and design multifunctional inorganic phases must first identify such equally important and property-determining "functional groups" or molecular units hiding in the crystalline state[2] and then subsequently establish methods to control and characterize their geometry and assembly.

Transition metal oxides of the ABO_3 perovskite class possess such a fundamental and functional unit: the corner-sharing BO_6 octahedra with central B-site transition metal cations coordinated by six oxygen ligands. Variations in the size (B–O bond lengths), shape (number of unequal B–O bonds), and connectivity (here used to describe the magnitude and pattern of octahedral rotations) of the functional octahedral units provide access to a wide spectrum of multifunctional properties (**Figure 1**), enabled by the strong coupling among the lattice, charge, spin, and orbital degrees of freedom.[3–5] Understanding the geometric patterns and tiling—symmetry and topology—of the BO_6 building blocks therefore permits material properties in perovskites to be explained in terms of their underlying structure, making these materials amenable to control for specific functionalities. One principal challenge

James M. Rondinelli, Materials Science and Engineering Department, Drexel University; jrondinelli@coe.drexel.edu
Steven J. May, Materials Science and Engineering Department, Drexel University; smay@coe.drexel.edu
John W. Freeland, X-ray Science Division, Argonne National Laboratory, USA; freeland@anl.gov
DOI: 10.1557/mrs.2012.49

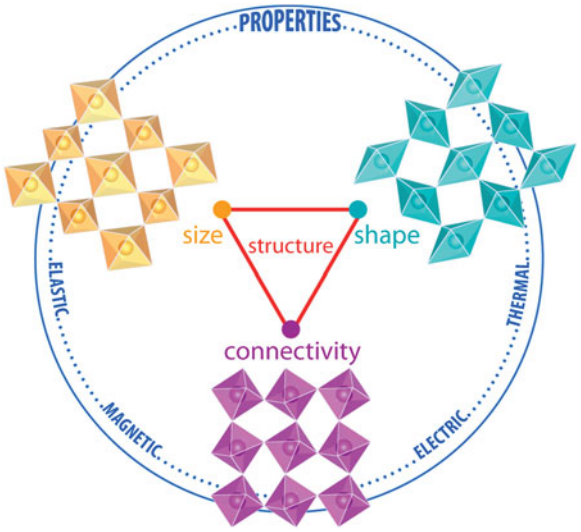

Figure 1. The interplay among different structural distortions of the octahedral units—their size, shape, and connectivity—dictates the functional elastic, magnetic, electric, and thermal properties.

to engineering functionality into perovskite oxides lies in finding new synthetic routes to control the crystal lattice. Studies of bulk systems have developed guidelines to understand perovskite structures based on ionic radii of the constituents and inter-atomic bond lengths (e.g., tolerance factor).[3] The strategy to control the size, shape, and connectivity of the BO_6 octahedra relies on hydrostatic pressure and/or chemical substitution/alloying; unfortunately, the octahedral responses are limited to the available chemistries. A grand challenge is then to find routes to go beyond this limitation to access multifunctional properties through rational control of the octahedral connectivity (i.e., the rotational patterns of the BO_6 units—the perovskite structural feature that has a profound impact on properties).

In this article, we describe how layer-by-layer epitaxial synthesis methods have opened the door to the direct tuning of the octahedral connectivity in perovskite oxides without resorting to chemical substitution. By building on the strong structure–property relationships in perovskites, epitaxial constraints provide new opportunities to achieve atomic and electronic structures that are inaccessible in bulk equilibrium phases. Using recent examples from the literature, we focus on three rapidly developing methods aimed at the targeted design of octahedral rotations (and their derived properties) in oxide thin films and heterostructures. These principal strategies are epitaxial strain, interfacial coupling at heterointerfaces, and coherent superlattice formation. We conclude by highlighting emerging avenues for both static/synthetic and dynamic external control of the octahedral connectivity in perovskite oxide heterostructures as a foundation for innovative technologies.

Function and structure of octahedra in perovskite oxides

Starting from a crystal-chemistry approach, the ABO_3 perovskite structure is built by tiling the fundamental BO_6 octahedral building blocks on the Cl sublattice in the simple interpenetrating cubic CsCl structure (**Figure 2**a) to yield the signature corner-connected BO_6 octahedral framework (Figure 2b). The A-site cations are then substituted on the Cs sites. In the absence of octahedral rotations and distortions, this creates the aristotype cubic perovskite phase with a three-fold axis along the body-diagonal.

The properties of most perovskite oxides are mainly attributed to the chemistry of the transition metal at the center of the BO_6 unit since the A-site cations prefer to form fixed valence, closed-shell electronic configurations. The electric, magnetic, and thermal responses depend on both the manner in which electrons fill the orbital levels on the B-site and on the covalency of the material,[6,7] a feature determined by the cation-oxygen bond lengths and the octahedral connectivity. The size, shape, and extended connectivity of the highly flexible octahedral framework (Figure 1) all modify the hybridization/chemical bonding through changes in the overlap of transition metal 3*d* and oxygen 2*p* orbitals.

The size of the BO_6 units can be modulated to form small and large octahedra without necessarily altering the point symmetry of the archetypal phase. For instance, static segregation of charge (δ) can drive an ordered charge disproportionation reaction of the type $2B^{N+} \rightleftharpoons B^{(N+\delta)+} + B^{(N-\delta)+}$ (N is the nominal ionic charge on the B cation),[8] which results in alternating octahedra that are dilated (long B–O bonds) and contracted (short B–O bonds) (Figure 1, left).[9,10] Shape-altering distortions of the octahedra can arise from the first-order cooperative Jahn-Teller effect when filling of B-site *d*-orbitals leads to an orbital degeneracy. The degeneracy can be lifted by tetragonally distorting the octahedra, where two elongated and four compressed B–O bonds are created (Figure 1, right).[11–13] Cooperative polar B-cation displacements can also occur and lead to noncentrosymmetric crystal structures with functional optical, piezo-, and ferroelectric properties.[14–16]

In addition to size and shape distortions, which modify the B–O bond lengths, rotations of the BO_6 units (Figure 1, bottom) buckle the octahedral framework along different Cartesian axes (B–O–B bond angles <180°) and play an important role in determining the physical properties of perovskite oxides. There are 15 distinct rotation patterns[17,18] that keep the BO_6 units nearly rigid and are classified using the Glazer notation[19] by the manner in which adjacent octahedra rotate along a particular Cartesian direction: $a^{-}(^{+})$ indicates out-of-phase (in-phase) rotations, while a^0 denotes no rotation, about a Cartesian axis. This is best illustrated for the simple case in Figure 2c, which shows in- and out-of-phase rotations only along the *z*-axis. For perovskite oxides, the cooperative behavior of the octahedra, reinforced by their corner connectivity, often results in two common rotation systems, rhombohedral ($a^{-}a^{-}a^{-}$) or orthorhombic ($a^{-}a^{-}c^{+}$) (Figure 2d).

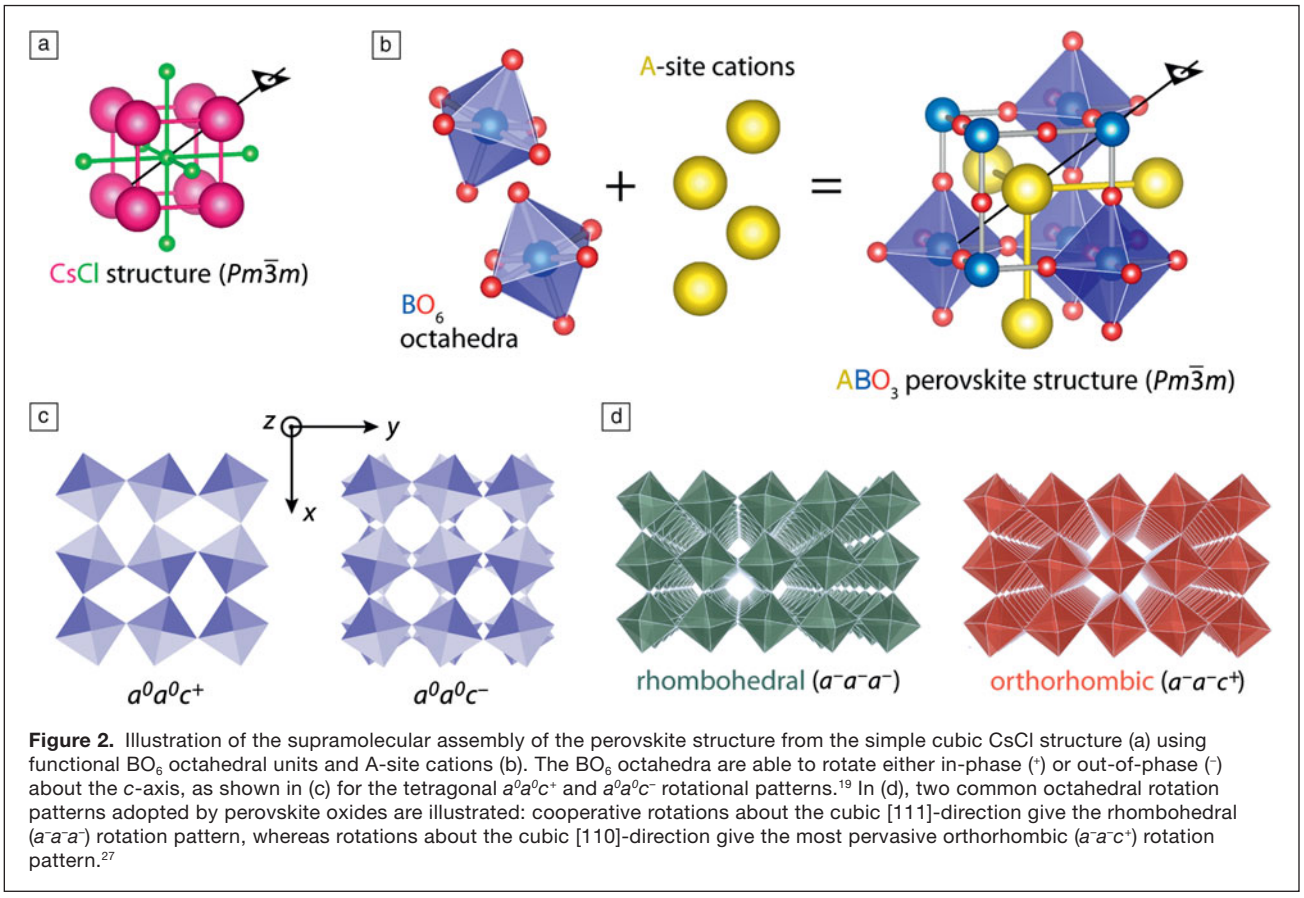

Figure 2. Illustration of the supramolecular assembly of the perovskite structure from the simple cubic CsCl structure (a) using functional BO_6 octahedral units and A-site cations (b). The BO_6 octahedra are able to rotate either in-phase ($^+$) or out-of-phase ($^-$) about the *c*-axis, as shown in (c) for the tetragonal $a^0a^0c^+$ and $a^0a^0c^-$ rotational patterns.[19] In (d), two common octahedral rotation patterns adopted by perovskite oxides are illustrated: cooperative rotations about the cubic [111]-direction give the rhombohedral ($a^-a^-a^-$) rotation pattern, whereas rotations about the cubic [110]-direction give the most pervasive orthorhombic ($a^-a^-c^+$) rotation pattern.[27]

These changes in the extended structure of the octahedral framework, which alter the translational symmetry, influence the material properties by bending the B–O–B bond angle away from 180°. The strength of the B–O–B interactions necessarily changes as the overlap between O 2*p* and B *d*-orbitals is reduced. The magnitude and symmetry of the rotations, for example, determine electronic bandgaps,[20] thermal conductivity,[21] magnetic properties,[22–24] and critical (superconductivity) transition temperatures.[25] They are most routinely controlled in bulk materials by judicious choice of the A- and B-site cation size mismatch[26–28] through chemical pressure[29–31] or through applications of external hydrostatic pressure.[32,33] **Figure 3** provides two examples of how isovalent A-site substitution is used to tune functional properties by altering the connectivity (B–O–B bond angles) of the functional BO_6 units in manganites[34,35] and nickelates.[36,37] However, this approach is limited by available chemistries. Finding new synthetic routes to tailor the connectivity of the octahedral building blocks in a manner independent of composition is highly desirable; it would provide directionality control over materials properties while simultaneously achieving desired compositions. Recent attention has been devoted to understanding epitaxial and heterostructure control of the octahedral rotations, generating structures with chemistries inaccessible via bulk synthesis.

Before strategies for octahedral control in films are discussed, we note that the measurement of oxygen positions in thin films, required to identify the octahedral behavior, presents a formidable task. In bulk perovskites, powder diffraction is available to characterize octahedral behavior, enabling identification of the structure-properties relationships shown in Figure 3. While x-ray diffraction is routinely used to gain insight into the shape and the size of the unit cell, the quantification of octahedral connectivity in films is much more difficult due to the limited sample volume of films, the presence of a thick substrate, and the weak scattering from oxygen atoms. However, advances in transmission electron microscopy and the availability of synchrotron x-ray sources have enabled measurements of rotational patterns and magnitudes in thin perovskite films.[38–47] These advances in experimental techniques concomitant with first-principles density functional methods have enabled new insights into octahedral behavior in oxide heterostructures.[47] More details on the application of density functional calculations to investigate structure in perovskite films can be found in a recently published review article.[48]

Strain engineering of octahedral rotations

For the last decade, the choice of substrate materials on which to grow a functional perovskite oxide has primarily been governed by the lattice mismatch between the substrate and film—an

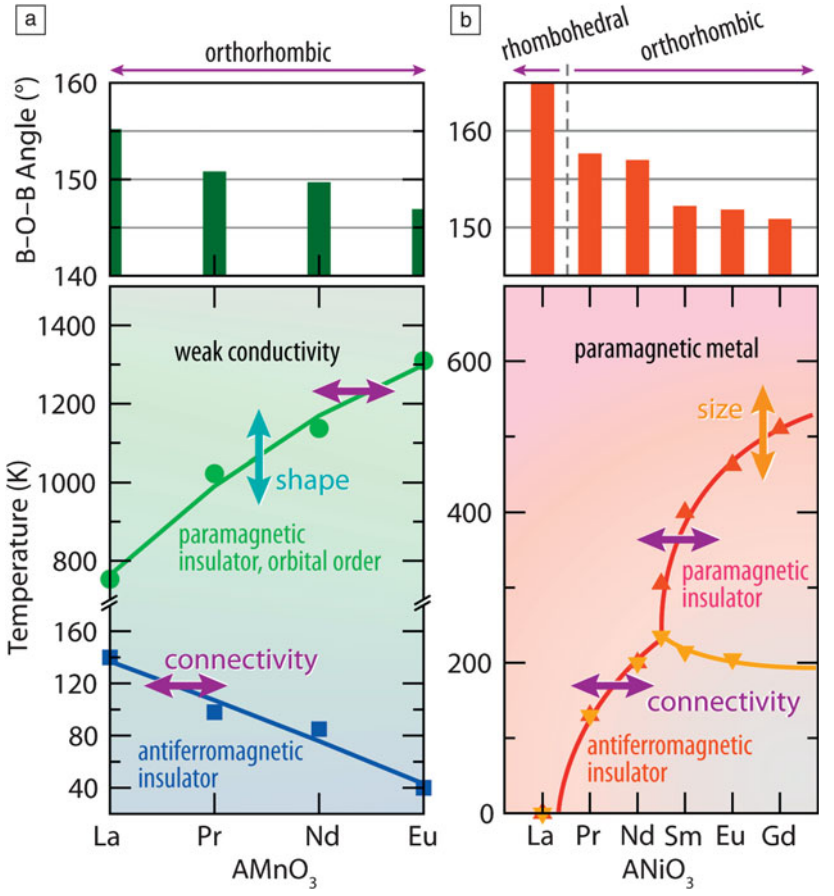

Figure 3. The isovalent phase diagrams of rare earth manganites (a) and nickelates (b) with A-site composition exhibit changes in the octahedral connectivity (B–O–B bond angles, upper panels) and symmetry. Changes to the octahedral connectivity (horizontal arrows) affect the temperatures associated with magnetic and charge ordering phase transitions, whereas periodic orderings of the octahedral shape and size (vertical arrows) occur at the orbital ordering and bond disproportionation transitions in the manganites and nickelates, respectively (lower panels). Data adapted from References 34–37.

approach taken from the growth and design of compound semiconductors. The underlying assumption in this strategy is that the elastic strain energy imposed on the film by the substrate is accommodated by changes in the film's unit cell parameters rather than by changes in the internal atomic positions. This route has been extremely successful in tailoring the dielectric, piezoelectric, and multiferroic properties of thin-film perovskites.[49–51]

However, the flexible corner-connected octahedral network in perovskites allows for epitaxial stresses to be accommodated by changes to octahedral connectivity (rotations), in addition to size and shape distortions. The strain–octahedral rotation coupling mechanism, however, is less understood and more poorly characterized than strain-induced lattice parameter distortions, due in part to the experimental difficulty in extracting oxygen positions in heteroepitaxial thin films. However, as octahedral rotations couple directly to magnetic, electronic, and multiferroic behaviors, strain-based control over these functional properties[52–60] requires a detailed understanding of the BO_6 units' response to epitaxial strain; it is the octahedral rotations and size/shape distortions, and not solely the lattice tetragonality (*c*/*a* ratio of in- versus out-of-plane lattice constants), that provide the physical basis for strain-induced changes to electronic and ferroic properties. To this end, first-principles density functional calculations[61,62] are proving to be particularly useful in revealing the coupling between strain and octahedral connectivity.[48]

Recent computational studies of rhombohedral perovskites with the $a^-a^-a^-$ pattern (Figure 2d) under biaxial strain show that strain directly modifies the magnitude of the octahedral rotations about different crystallographic directions relative to that of the substrate.[39,63] **Figure 4**a shows that in $LaAlO_3$, compressive biaxial strain enhances the magnitude of the octahedral rotations about the [001]-direction, while tensile strain favors the [110]-direction (i.e., in-plane octahedral rotations).[63] In fact, moderately large compressive (tensile) strains are able to completely quench the rotations about the [110] ([001]) axis, achieving atomic configurations inaccessible in the bulk. For small intermediate strains, the bulk-like rotation pattern persists, albeit with a small monoclinic distortion of the lattice.

In rhombohedral $LaNiO_3$, however, the strain-space over which the bulk-like rhombohedral rotation phase persists is much larger. It is stable for all computationally explored strain values.[39] Nonetheless, distinct changes in the electronic conductivity are observed.[64,65] This occurs because the misfit strain directly alters both the octahedral shape and connectivity (Figure 4b–c). Somewhat unexpectedly at first glance, the *in-plane* bond angles are weakly sensitive to the epitaxial strain state, while the out-of-plane bond angle can be tuned by nearly 3.6° per percent strain. In contrast, the in-plane bond lengths couple linearly to strain—a consequence of accommodating the change in the in-plane unit cell area that occurs from coherent epitaxy—while the out-of-plane bond lengths are weakly dependent on strain. The latter occurs because the changes in the out-of-plane lattice parameter (due to Poisson effects) are accommodated largely by the rotations of the octahedra rather than through bond compression. Using an x-ray diffraction approach based on the measurement of half-order peaks arising from octahedral rotations,[66] the rotational magnitudes in strained $LaNiO_3$ films were measured and found to be in good agreement with the first-principles results described previously.[39] Similarly, in films of $La_{0.5}Sr_{0.5}CoO_3$, which is rhombohedral in bulk form, extended x-ray absorption spectroscopy (EXAFS) was used

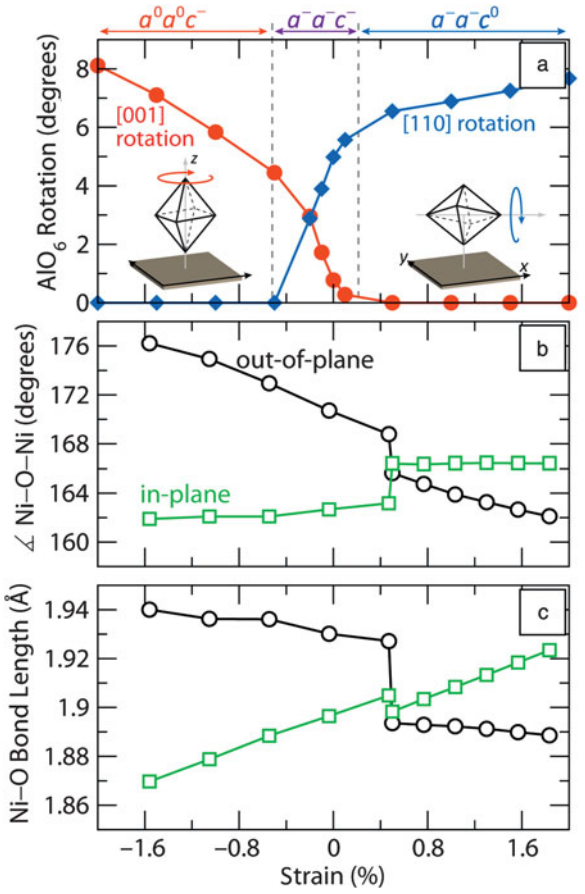

Figure 4. The zero-kelvin density functional theory (local density approximation) strain–octahedral phase diagram for rhombohedral $LaAlO_3$ under biaxial strain (a). The choice of lattice mismatch between the film and substrate enables selection of the thin film's octahedral rotation angles: Increasing strain from compressive to tensile changes the magnitude of the AlO_6 rotation angles about the different Cartesian directions $a^0a^0c^-$, (along *z*-) $a^-a^-c^-$ (along *x*-, *y*-, and *z*-), and $a^-a^-c^0$ (along *x*- and *y*-directions) relative to the (001)-oriented cubic substrate (inset). The simulated (001)-strain dependence on the in-plane (□) and out-of-plane (○) bond angles (b) and bond lengths (c) for rhombohedral $LaNiO_3$ reveal that strain is accommodated by octahedral rotations and transition metal bond distortions. Data reproduced from References 48 and 63. ©2010, American Physical Society and ©2011, Wiley-VCH Verlag.

to show that strain is accommodated by both octahedral rotations and distortions.[67]

In addition, epitaxial control of octahedral rotations provides a new opportunity to realize novel phase transitions: the discontinuity near 0.5% strain in Figure 4b–c signals an isosymmetric transition[68] that is associated with the change in "sense" of the $a^-a^-c^-$ rotation pattern, which occurs when the film's axial (*c*/*a*) ratio approaches unity. Such structure-driven transitions are inaccessible in bulk rhombohedrally distorted perovskites since they originate from the 2D-mechanical coupling of the octahedral framework of the film to the substrate. These abrupt (isosymmetric) transitions[69] in octahedral rotation patterns were recently reported near the self-morphotropic phase boundary in highly compressed magnetoelectric and multiferroic $BiFeO_3$ films.[70] At this functional transition—accessible only through misfit strain control—a concomitant large and electric-field-tunable[71] reorientation of the ferroelectric polarization occurs.

Orthorhombic perovskites offer the ability to separately control the B–O bond lengths and B–O–B angles because they have an intrinsic or "built-in" anisotropy originating from the $a^-a^-c^+$ rotation pattern (Figure 2d) not afforded by their rhombohedral relatives. The in-phase component (c^+) of the rotation pattern occurs about the longest axis. Thus, control over electric and magnetic polarizations[72–75] is predicted to be accessible by judiciously choosing the film/substrate orientation. In *c*-oriented orthorhombic $SrRuO_3$ films (i.e., with the c^+ rotation about the long axis set perpendicular to the substrate) the rotation–strain interactions resemble those described for rhombohedral perovskites. Compressive (tensile) strain increases (decreases) the rotations about the [001]-direction, while the total magnitude of the rotation pattern is kept nearly constant by a compensating increase (decrease) in the rotations about the [110]-direction. In films where the long axis and the c^+ rotation occurs in the plane of epitaxy, however, *both* rotations about the [001] and [110]-directions decrease as the strain goes from compressive to tensile.[76] Controlled growth of orthorhombic perovskites should therefore enable a direct route for tuning the total magnitude of the rotational pattern—the B–O–B bond angles and thus the magnetic interactions and electronic bandwidths derived from them. Indeed, the asymmetric orientation-dependent RuO_6 rotation response in $SrRuO_3$ films was found to give a larger magnetostructural coupling than that provided by biaxial strain alone.[77]

Clearly, strain couples strongly to octahedral rotations in perovskite oxides. A substantial portion of the change in lattice parameters is mediated by changes in both the relative magnitude of the BO_6 octahedral rotations and the B–O bond lengths. Complete guidelines governing the response of the octahedral units in perovskites to strain are not yet available; however, these early studies reveal that misfit strain provides a direct handle by which to tune a film's octahedral rotational patterns and properties.

Interfacial coupling of octahedral rotations

The substrate also plays a crucial role in determining the octahedral behavior of the film. In addition to imposing mechanical stresses and epitaxial strain on the film, perovskite-structured substrates also enforce a geometric constraint: the BO_6 octahedra (barring oxygen vacancies) must remain corner-connected. This corner-connectivity enables the octahedral distortions and rotations present in the substrate to be transferred across the heteroepitaxial interface and imprinted into the film. In other words, there exists an octahedral proximity effect at perovskite/perovskite heterointerfaces (**Figure 5**).[78–80]

Interfacial octahedral coupling provides a complementary route to the strain coupling described previously for tuning the connectivity of the functional BO_6 units.[41,78–81] Symmetry

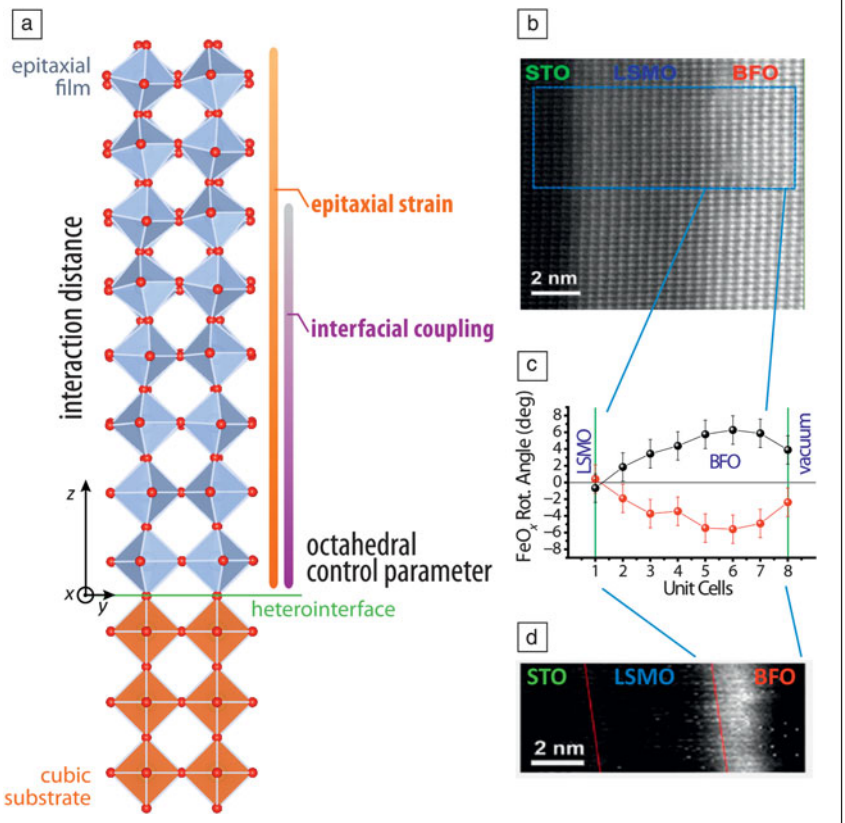

Figure 5. A schematic illustration detailing how rotations in a film ($a^-a^-c^-$ pattern) might evolve with distance from a cubic substrate due to different octahedral control parameters (structural tuning knobs: epitaxial strain and/or interfacial coupling) (a). Interfacial octahedral coupling effects have been observed at a $BiFeO_3/La_{0.7}Sr_{0.3}MnO_3$ interface (b), in which the rotation angles of the FeO_6 octahedra (odd [red] and even [black] sites of the two-dimensional map) are suppressed at the heterointerface (c). The reduced rotations lead to a near interfacial region that exhibits an anomalous dielectric response, as indicated by the non-linear behavior of the low energy component of the electron energy loss spectra (d, showing the χ^2-error [weighted sum of squared errors] of the multiple linear least squares fit). Parts (b and d) reproduced from and part (c) adapted from Reference 78. ©2010, American Physical Society. Note: BFO, $BiFeO_3$; LSMO, $La_{0.7}Sr_{0.3}MnO_3$; and STO, $SrTiO_3$.

matching between the film and substrate has been shown to play a key role in stabilizing high-quality perovskite films.[82] However, the intentional use of a symmetry-mismatch between the substrate and film allows for the stabilization of non-equilibrium rotational patterns in the films. For example, rotations present in the low temperature, tetragonal phase of a $SrTiO_3$ substrate were predicted to persist into a $SrFeO_3$ film, creating an interfacial region with a symmetry that differs from bulk cubic $SrFeO_3$.[79] Interfacial coupling not only modifies the octahedral response of the film, but it can also modify the atomic structure within the substrate at the heterojunction. In the $SrTiO_3/LaAlO_3$ system, scanning transmission electron microscopy (STEM) imaging revealed that the bulk-like ($a^-a^-a^-$) octahedral rotations present in the $LaAlO_3$ film propagate into a cubic (lacking rotations at room temperature) $SrTiO_3$ substrate, altering the $SrTiO_3$ symmetry in the three unit cells nearest the interface.[41]

The octahedral coupling across a perovskite heterointerface may allow for the stabilization of different lattice symmetries in films under nearly identical strain states—an inaccessible route to tailor functionality in structurally simple binary oxides and compound semiconductors. For example, consider an ultrathin rhombohedral ($a^-a^-a^-$) film grown epitaxially on cubic $(La_{1-x}Sr_x)(Al_{1-y}Ta_y)O_3$ (LSAT) ($a^0a^0a^0$) and orthorhombic $NdGaO_3$ ($a^-a^-c^+$) substrates, two crystals with similar pseudocubic lattice parameters.[48] Each substrate may stabilize octahedral rotation patterns at the film/substrate interface that are absent in the rhombohedral film's bulk phase. Full control of the octahedral proximity effect in this capacity remains to be exploited for realizing multifunctional heterostructures.

Interfacial octahedral coupling also provides a direct and controllable route to alter the BO_6 rotation angles at the heterointerface. In situations where a rhombohedral or orthorhombic film is grown on a cubic substrate, the substrate is able to largely suppress rotations in the near interface region of the film. At the interfaces between the cubic phase of $SrTiO_3$ and rhombohedral $La_{0.75}Sr_{0.25}MnO_3$ ($a^-a^-c^-$), the rotations about the [110]-direction are quenched in the manganite, while the rotations about the [001] direction are slightly enhanced.[80] A similar interfacial behavior was reported for the case of orthorhombic $SrRuO_3$ ($a^-a^-c^+$) on $SrTiO_3$.[80,83]

The altered connectivity of the BO_6 units in the interfacial region should exhibit electronic and/or ferroic behavior that differs from the non-interfacial regions of the film and its bulk counterpart. For instance, the suppression of rotations can lead to interfacial regions with anomalous dielectric behavior and a reduced bandgap, as was observed in the near-interfacial region of $BiFeO_3$ at the $BiFeO_3/La_{0.7}Sr_{0.3}MnO_3/SrTiO_3$ heterointerface (Figure 5b–d).[78] In addition to static octahedral reconstructions, the lattice vibrational (phonons) modes associated with dynamic octahedral rotations (cooperative oxygen displacements) can propagate across interfaces and produce markedly different macroscopic electronic properties. Coupling of the phonons associated with the $a^0a^0c^-$ pattern in the $SrTiO_3$ substrate was found to increase the resistivity of an $La_{0.53}Sr_{0.47}MnO_3$ film due to enhanced phonon scattering at temperatures near the cubic-to-tetragonal $SrTiO_3$ structural phase transition.[84] This phase transition also produces long-range buckling of the $SrTiO_3$ surface leading to anisotropic surface rumpling, a structural feature that can propagate into epitaxial films.[81,85]

An important aspect of engineering the octahedral proximity effect is the spatial length scale over which the octahedral patterns in the film are modified, because this is the region

accessible to property control via the functional BO_6 units. Although the precise distance over which the substrate-induced rotational behavior penetrates across the interface remains an open issue, early evidence suggests it is determined by the symmetries of the rotational patterns belonging to the bulk phases of the substrate and film, as well as the chemical mismatch between these materials. For instance, density functional techniques have shown that the single-axis rotations imprinted from insulating $SrTiO_3$ into metallic $SrFeO_3$ persist for only two unit cells about the [001]-direction,[79] likely a result of the weak interlayer coupling associated with the $a^0a^0c^-$ rotations about that *z*-direction (i.e., this rotation pattern maintains corner-connectivity across the interface independent of the rotations about the [001] direction). When the coupling involves both in- and out-of-plane rotations, however, the substrate-induced behavior is expected to persist over greater length scales. Altered octahedral behavior is reported over a five unit cell region (~2 nm) at the $SrTiO_3/La_{0.75}Sr_{0.25}MnO_3$ interface.[80] A similar length scale was observed with STEM for the suppression of rotations in $BiFeO_3$ at a heterojunction with $La_{0.7}Sr_{0.3}MnO_3$.[78] Films of $SrRuO_3$ grown on $SrTiO_3$ were found to exhibit a tetragonal symmetry for at least 9 unit cells before relaxing to their bulk-like orthorhombic symmetry at greater film thicknesses, suggesting that interfacial-stabilized symmetries persist over more than just a few unit cells.[83] The strength and length scale of interfacial octahedral coupling at structurally more complex rhombohedral/orthorhombic ($[a^-a^-a^-]/[a^-a^-c^+]$) heterointerfaces, two of the most commonly occurring symmetries in perovskites, remain to be explored.

Coherent heteroepitaxy of perovskite films requires the BO_6 octahedra to both distort and rotate to maintain the corner-connected network across the substrate-film heterojunction. This requirement provides an opportunity to tailor the interfacial coupling of BO_6 octahedral behavior to stabilize familiar perovskite materials with new functionalities. To effectively harness this effect requires that both the lattice parameters and symmetry of the substrate are fully considered during experimental design and analysis in addition to the processes—changes in bond lengths and bond angles and/or point and planar defect formation—by which the octahedral behavior in the film relaxes away from the substrate-induced symmetry. One important area of future study is developing a deeper understanding of the local structure in the region where the interfacial coupling effect yields to the epitaxial strain-rotation coupling—local octahedral distortions are likely required to maintain the geometric connectivity.[78] A greater understanding of the role played by the electronic structure of the two materials—whether a metal/metal, insulator/metal, or insulator/insulator heterointerface exists—is also likely a critical aspect to realizing the full potential of this design approach.

Rotational behavior in synthetic superlattices

The octahedral proximity effect identified at the substrate/film interface can be additionally exploited for rational control of the BO_6 octahedral units in ways not available to single layer films or simple heterojunctions. The formation of short-period coherent superlattices and multilayer heterostructures—consisting of two materials with different transition metal cations (B and B') and dissimilar BO_6 and $B'O_6$ rotational symmetries and/or magnitudes at a periodicity shorter than the length scale associated with relaxation of the proximity effect—makes it possible to either (1) maximize the interfacial octahedral coupling effect in short-period superlattices, or (2) spatially localize the non-equilibrium octahedral behavior, realizing a form of rotational "δ-doping," described more thoroughly later. Both routes afford control of the octahedral behavior in synthetic heterostructures through changes in the relative number of constituent repeat units (and their composition) in the heterostructure—parameters selected prior to materials synthesis and thus amenable to rational property design.

Tuning the ratio of the BO_6 and $B'O_6$ octahedra in a superlattice provides direct control over the octahedral shape and connectivity in a fundamentally different fashion than that available to simple fixed-composition and epitaxially strained films. Consider, for example, different period (*n,m*)-superlattices formed from cubic (*n*) and rhombohedral (*m*) perovskites with the $a^0a^0a^0$ and $a^-a^-c^-$ patterns (**Figure 6**a), respectively. The overall superlattice composition derived from the number of *n* and *m* building blocks, given as $C = n/(n+m)$, emerges as a new variable to tune the octahedral connectivity through the proximity effect. Increasing the composition $C \rightarrow 1$ at fixed *m,* for example, favors the non-tilted octahedral geometry. The proximity effect derived from the cubic perovskites blocks (*n*) suppresses the preference for rotations in the rhombohedral (*m*) blocks. As a result, *all* inter-octahedral B–O–B bond angles increase toward 180° in the superlattice (Figure 6b). This is unlike the strain–octahedral rotation coupling where a decrease (increase) in the in-plane bond angle is usually accommodated by an increase (decrease) in the out-of-plane bond angle (Figure 6c), thereby maintaining the net magnitude of the octahedral rotation system as nearly constant. The compositional control in the superlattice enables a net reduction or enhancement in the total rotation amplitude. Due to the corner-connectivity of the perovskite structure, this net change in octahedral rotation magnitude forces cooperative compression (or elongation) of all B–O bonds (Figure 6d), contrasting the compensating and anisotropic behavior observed in strained films (Figure 6e).

This tuning of the bond lengths and angles through superlattice composition control has recently been demonstrated in $(LaNiO_3)_m/(SrMnO_3)_2$ superlattices.[86] For superlattices with $m = 1$, the rotations are strongly suppressed ($SrMnO_3$ is cubic) and yields ultrathin nickelate layers exhibiting octahedral behavior that is markedly different from the bulk—the NiO_6 rotations are almost completely absent. In contrast, large rotations are induced in the $SrMnO_3$ layers for the case of $m = 4$. As a result, direct tuning of structure-driven electronic properties should be accessible using this superlattice approach. Indeed, variable composition $SrTiO_3/SrFeO_3$ superlattices exhibit remarkably different octahedral size, shape, and connectivity

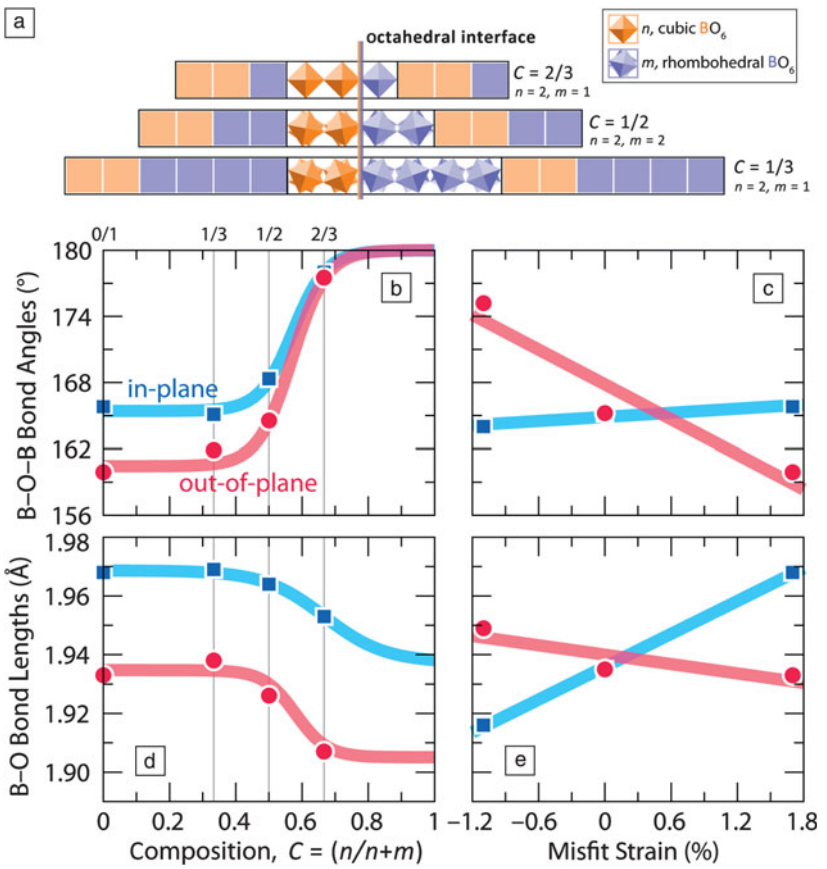

Figure 6. A schematic illustrating octahedral rotational control in short-period perovskite superlattices consisting of cubic and rhombohedral constituents of varying thickness (a). In (b and c), the bond angles in $(SrMnO_3)_n/(LaNiO_3)_m$ superlattices and strained $LaNiO_3$ films are compared showing the distinct octahedral responses to superlattice formation at varying composition (left panels) and epitaxial strain at fixed composition (right panels). The behavior of the B–O bond lengths for the same set of superlattices and films are shown in (d and e). Altering the superlattice composition makes it possible to decrease (or increase) both the in-plane and out-of-plane structural features simultaneously; in contrast, a decrease (increase) of an in-plane structural feature from epitaxial strain is compensated by an increase (decrease) in the corresponding out-of-plane feature. Data adapted from References 35 and 86. Note: *C*, overall superlattice composition.

with corresponding metal-insulator transitions and orbital polarizations.[87] First-principles calculations of $LaNiO_3/LaAlO_3$ superlattices also reveal a strong coupling between the electronic structure and octahedral behavior.[88] Furthermore, the formation of ultrashort $n = m = 1$ superlattices with perovskite constituents that have different octahedral rotations patterns appears to be an emerging strategy for realizing novel forms of improper ferroelectricity (i.e., the primary order parameter for the phase transition is not the ferroelectric polarization).[89] A polarization enhancement occurs in ultrashort 1/1 period $SrTiO_3/PbTiO_3$ superlattices simultaneously with a modulation in the $a^0a^0c^-$ rotation magnitude in $SrTiO_3$ from the heterointerface proximity effect with $PbTiO_3$.[47] Such unusual forms of ferroelectricity are crucial for realizing temperature-independent dielectric properties for thin-film capacitor applications.

The unit cell-by-unit cell growth of oxide heterostructures allows for δ-doping of chemically and structurally distinct single BO_6 monolayers. These approaches, which were originally employed in conventional semiconductor heterostructures,[90] are actively being pursued in perovskite oxides as a route to enhance carrier mobility and tune magnetic interactions.[91–93] Using the rotational proximity effect in a digitally ordered superlattice allows a perovskite, which exhibits large octahedral rotations in the bulk, to be sandwiched within a material with no tendency to rotations (i.e., $n \gg m$, $m = 1$). The spatially confined BO_6 rotation layer, or δ-doped rotation, which occurs simultaneously with A-site cation substitution, enables direct charge-carrier doping and electronic control in the octahedrally doped region. This strategy was recently demonstrated in a series of uniformly strained $SrTiO_3/LaAlO_3$ heterojunctions, interleaved with different single layer $A^{3+}AlO_3$ unit cells with larger octahedral rotations (decreasing rare-earth ionic radii), to be a remarkably powerful route to tune a metal-insulator transition in a buried two-dimensional electron gas.[94]

Another intriguing line of study made possible by these octahedral engineering approaches is the formation of rotational superstructures that exhibit spatially modulated rotational magnitudes or rotational periods much longer than two unit cells. Such a structure could be realized in superlattices by tuning the constituent layer thicknesses, allowing partial relaxation of the octahedral rotations between the interfaces. These superstructures may give rise to novel modulated magnetic and electronic behavior. Additionally, the importance of covalent interactions in perovskites for stabilizing rotational patterns[95] suggests that the formation of artificially structured oxides in which the constituent compounds exhibit dramatically different electronic structures could yield novel octahedral behavior. The abrupt changes in covalency among the chemically distinct layers could be used to realize particular rotation patterns and, in turn, desired material properties.

Summary and prospects

Tailoring the size, shape, and connectivity of functional BO_6 units is crucial to engineering material properties in perovskites. The thermal, electric, and magnetic responses are all strongly linked to changes in the atomic structure. We have illustrated the principal routes by which direct control over the connectivity of the octahedral structure is possible using epitaxial constraints. This offers exciting opportunities to achieve desired properties in targeted compositions and the possibility of generating new

ground-states unavailable in the bulk counterparts. However, a multifunctional material should be responsive to a variety of external stimuli (e.g., pressure, strain, chemical, optical, electric, and magnetic). The direct routes we have described for tuning the octahedral connectivity make it possible to position many transition metal perovskite oxides closer to functional phase boundaries where external perturbations may be used to traverse and induce colossal responses.

Consider the case of coupling to external electric fields, especially in lieu of the desire to utilize complex transition metal oxides as low-power electronic materials,[96] where the property-determining rotations should be electric-field addressable. In simple perovskites, the individual octahedra and their broader connectivity couple weakly (if at all) to external electric fields—a consequence of the geometric centricity of the BO_6 units. This raises a critical challenge for the discovery of new multifunctional electric-field tunable oxides: Are there synthetic perovskite assembly routes that permit combinations of BO_6 octahedra to induce polarizations? Such questions are intensely being studied, and materials design guidelines for engineering BO_6 octahedra that respond to electric fields are at present being identified;[47,89,97–99] quasi-two dimensionality or "layering" achieved through A-site cation ordering *and* particular orthorhombic rotation systems appear promising. Strategies for external control of rotations may also arise from a recently developed system for describing rotational symmetry operations.[100] Another route to control the octahedral rotations relies on the piezoelectric effect in heterostructures integrating piezoelectric substrates or interfacial layers:[101] Application of an electric field induces a lattice distortion, which modifies the strain state, and in turn the octahedral rotation magnitudes through strain–rotation coupling. Additional opportunities for dynamical control of structure arise from photostriction[102] or harnessing direct phonon coupling with THz radiation.[103,104]

To fully exploit these emerging design approaches requires addressing several fundamental questions: What are the critical parameters that determine the octahedral behavior in a film under epitaxial strain or across a heterointerface with a symmetry mismatch? What are the length scales and mechanisms associated with relaxation of substrate-induced octahedral behavior? To what extent is it possible to separate cation composition and material symmetry? How can octahedral behavior be controlled independently along both in-plane and out-of-plane directions? How do defects inhibit the strategies described herein to control octahedral connectivity? We anticipate that great strides will be made in addressing these questions over the next decade, and in the process, materials scientists will establish new strategies for structure-driven control of functional properties in complex oxide heterostructures.

Acknowledgments

The authors would like to acknowledge fruitful discussions with K.R. Poeppelmeier, C.J. Fennie, P.M. Woodward, D.D. Fong, P.J. Ryan, and A.Y. Borisevich. S.J.M. and J.M.R. gratefully acknowledge support from the Office of Naval Research (ONR N00014–11–1-0664). J.W.F. was supported by the U.S. DOE, Basic Energy Sciences, under U.S. DOE, Office of Basic Energy Sciences, under Contract No. DE-AC02–06CH11357.

References

1. D.R. Kanis, M.A. Ratner, T.J. Marks, *Chem. Rev.* **94**, 195 (1994).
2. R. Hoffmann, *Solids and Surfaces: A Chemist's View of Bonding in Extended Structures* (VCH, New York, 1988).
3. J.B. Goodenough, *Rep. Prog. Phys.* **67**, 1915 (2004).
4. M.B. Salamon, M. Jaime, *Rev. Mod. Phys.* **73**, 583 (2001).
5. M. Imada, A. Fujimori, Y. Tokura, *Rev. Mod. Phys.* **70**, 1039 (1998).
6. J.B. Goodenough, *J. Appl. Phys.* **37**, 1415 (1966).
7. J. Zaanen, G.A. Sawatzky, J.W. Allen, *Phys. Rev. Lett.* **55**, 418 (1985).
8. I.I. Mazin, D.I. Khomskii, R. Lengsdorf, J.A. Alonso, W.G. Marshall, R.A. Ibberson, A. Podlesnyak, M.J. Martinez-Lope, M.M. Abd-Elmeguid, *Phys. Rev. Lett.* **98**, 176406 (2007).
9. T. Takeda, R. Kanno, Y. Kawamoto, M. Takano, S. Kawasaki, T. Kamiyama, F. Izumi, *Solid State Sci.* **2**, 673 (2000).
10. P.M. Woodward, D.E. Cox, E. Moshopoulou, A.W. Sleight, S. Morimoto, *Phys. Rev. B* **62**, 844 (2000).
11. H.A. Jahn, E. Teller, *Proc. R. Soc. London, Ser. A* **161**, 220 (1937).
12. J.B. Goodenough, *Annu. Rev. Mater. Sci.* **28**, 1 (1998).
13. M.W. Lufaso, P.M. Woodward, *Acta Crystallogr., Sect. B: Struct. Sci.* **60**, 10 (2004).
14. J.K. Burdett, *Inorg. Chem.* **20**, 1959 (1981).
15. M. Kunz, I.D. Brown, *J. Solid State Chem.* **115**, 395 (1995).
16. P.S. Halasyamani, K.R. Poeppelmeier, *Chem. Mater.* **10**, 2753 (1998).
17. C.J. Howard, H.T. Stokes, *Acta Crystallogr., Sect. B: Struct. Sci.* **54**, 782 (1998).
18. H.T. Stokes, E.H. Kisi, D.M. Hatch, C.J. Howard, *Acta Crystallogr., Sect. B: Struct. Sci.* **58**, 934 (2002).
19. A.M. Glazer, *Acta Crystallogr., Sect. B: Struct. Sci.* **28**, 3384 (1972).
20. H.W. Eng, P.W. Barnes, B.M. Auer, P.M. Woodward, *J. Solid State Chem.* **175**, 94 (2003).
21. Y. Wang, Y. Sui, P. Ren, L. Wang, X.J. Wang, W.H. Su, H.J. Fan, *Inorg. Chem.* **49**, 3216 (2010).
22. P.W. Anderson, *Phys. Rev.* **79**, 350 (1950).
23. J.B. Goodenough, *Phys. Rev.* **100**, 564 (1955).
24. J. Kanamori, *J. Appl. Phys.* **31**, 14S (1960).
25. S. Pei, J.D. Jorgensen, B. Dabrowski, D.G. Hinks, D.R. Richards, A.W. Mitchell, J.M. Newsam, S.K. Sinha, D. Vaknin, A.J. Jacobson, *Phys. Rev. B* **41**, 4126 (1990).
26. P.M. Woodward, *Acta Crystallogr., Sect. B: Struct. Sci.* **53**, 32 (1997).
27. P.M. Woodward, *Acta Crystallogr., Sect. B: Struct. Sci.* **53**, 44 (1997).
28. V.M. Goldschmidt, *Naturwissenschaften* **14**, 477 (1926).
29. Y. Tomioka, Y. Tokura, *Phys. Rev. B* **70**, 014432 (2004).
30. J.B. Torrance, P. Lacorre, A.I. Nazzal, E.J. Ansaldo, C. Niedermayer, *Phys. Rev. B* **45**, 8209 (1992).
31. N.W. Thomas, *Acta Crystallogr., Sect. B: Struct. Sci.* **52**, 16 (1996).
32. R.J. Angel, J. Zhao, N.L. Ross, *Phys. Rev. Lett.* **95**, 025503 (2005).
33. T. Tohei, A. Kuwabara, T. Yamamoto, F. Oba, I. Tanaka, *Phys. Rev. Lett.* **94**, 035502 (2005).
34. J.-S. Zhou, J.B. Goodenough, *Phys. Rev. B* **68**, 144406 (2003).
35. B. Dabrowski, S. Kolesnik, A. Baszczuk, O. Chmaissem, T. Maxwell, J. Mais, *J. Solid State Chem.* **178**, 629 (2005).
36. J.S. Zhou, J.B. Goodenough, B. Dabrowski, P.W. Klamut, Z. Bukowski, *Phys. Rev. Lett.* **84**, 526 (2000).
37. M.L. Medarde, *J. Phys. Condens. Matter* **9**, 1679 (1997).
38. C.K. Xie, J.I. Budnick, W.A. Hines, B.O. Wells, J.C. Woicik, *Appl. Phys. Lett.* **93**, 182507 (2008).
39. S.J. May, J.W. Kim, J.M. Rondinelli, E. Karapetrova, N.A. Spaldin, A. Bhattacharya, P.J. Ryan, *Phys. Rev. B* **82**, 014110 (2010).
40. F. He, B.O. Wells, S.M. Shapiro, *Phys. Rev. Lett.* **94**, 176101 (2005).
41. C.L. Jia, S.B. Mi, M. Faley, U. Poppe, J. Schubert, K. Urban, *Phys. Rev. B* **79**, 081405R (2009).
42. A. Vailionis, H. Boschker, W. Siemons, E.P. Houwman, D.H.A. Blank, G. Rijnders, G. Koster, *Phys. Rev. B* **83**, 064101 (2011).
43. A. Borisevich, O.S. Ovchinnikov, H.J. Chang, M.P. Oxley, P. Yu, J. Seidel, E.A. Eliseev, A.N. Morozovska, R. Ramesh, S.J. Pennycook, S.V. Kalinin, *ACS Nano* **4**, 6071 (2010).
44. Y. Han, I.M. Reaney, R.L. Johnson-Wilke, M.B. Telli, D.S. Tinberg, I. Levin, D.D. Fong, T.T. Fister, S.K. Streiffer, S. Trolier-McKinstry, *J. Appl. Phys.* **107**, 123517 (2010).
45. A. Miniotas, A. Vailionis, E.B. Svedberg, U.O. Karlsson, *J. Appl. Phys.* **89**, 2134 (2001).
46. Y. Wakabayashi, *Journal of Physics: Condensed Matter* **23**, 483001 (2011).
47. D.A. Muller, *Nat. Mater.* **8**, 263 (2009).

48. J.M. Rondinelli, N.A. Spaldin, *Adv. Mater.* **23**, 3363 (2011).
49. R. Ramesh, D.G. Schlom, *Mater. Res. Soc. Bull.* **33**, 1006 (2008).
50. S.K. Streiffer, D.D. Fong, *Mater. Res. Soc. Bull.* **34**, 832 (2009).
51. D.G. Schlom, L.-Q. Chen, C.-B. Eom, K.M. Rabe, S.K. Streiffer, J.M. Triscone, *Annu. Rev. Mater. Res.* **37**, 589 (2007).
52. C. Thiele, K. Dorr, O. Bilani, J. Rodel, L. Schultz, *Phys. Rev. B* **75**, 054408 (2007).
53. C. Adamo, X. Ke, H.Q. Wang, H.L. Xin, T. Heeg, M.E. Hawley, W. Zander, J. Schubert, P. Schiffer, D.A. Muller, L. Maritato, D.G. Schlom, *Appl. Phys. Lett.* **95**, 112504 (2009).
54. J.H. Lee, L. Fang, E. Vlahos, X.L. Ke, Y.W. Jung, L.F. Kourkoutis, J.W. Kim, P.J. Ryan, T. Heeg, M. Roeckerath, V. Goian, M. Bernhagen, R. Uecker, P.C. Hammel, K.M. Rabe, S. Kamba, J. Schubert, J.W. Freeland, D.A. Muller, C.J. Fennie, P. Schiffer, V. Gopalan, E. Johnston-Halperin, D.G. Schlom, *Nature* **466**, 954 (2010).
55. J. Liu, M. Kareev, B. Gray, J.W. Kim, P. Ryan, B. Dabrowski, J.W. Freeland, J. Chakhalian, *Appl. Phys. Lett.* **96**, 233110 (2010).
56. Y. Takamura, R.V. Chopdekar, E. Arenholz, Y. Suzuki, *Appl. Phys. Lett.* **92**, 162504 (2008).
57. F.J. Wong, S.H. Baek, R.V. Chopdekar, V.V. Mehta, H.W. Jang, C.B. Eom, Y. Suzuki, *Phys. Rev. B* **81**, 161101(R) (2010).
58. D. Okuyama, M. Nakamura, Y. Wakabayashi, H. Itoh, R. Kumai, H. Yamada, Y. Taguchi, T. Arima, M. Kawasaki, Y. Tokura, *Appl. Phys. Lett.* **95**, 152502 (2009).
59. Y. Suzuki, H.Y. Hwang, S.W. Cheong, R.B. van Dover, *Appl. Phys. Lett.* **71**, 140 (1997).
60. H. Boschker, M. Mathews, E.P. Houwman, H. Nishikawa, A. Vailionis, G. Koster, G. Rijnders, D.H.A. Blank, *Phys. Rev. B* **79**, 214425 (2009).
61. P. Hohenberg, W. Kohn, *Phys. Rev.* **136**, B864 (1964).
62. W. Kohn, L.J. Sham, *Phys. Rev.* **140**, A1133 (1965).
63. A.J. Hatt, N.A. Spaldin, *Phys. Rev. B* **82**, 195402 (2010).
64. J. Son, P. Moetakef, J.M. LeBeau, D. Ouellette, L. Balents, S.J. Allen, S. Stemmer, *Appl. Phys. Lett.* **96**, 062114 (2010).
65. J. Chakhalian, J.M. Rondinelli, J. Liu, B.A. Gray, M. Kareev, E.J. Moon, N. Prasai, J. L. Cohn, M. Varela, I.C. Tung, M.J. Bedzyk, S.G. Altendorf, F. Strigari, B. Dabrowski, L.H. Tjeng, P.J. Ryan, J.W. Freeland, *Phys. Rev. Lett.* **107**, 116805 (2011).
66. A.M. Glazer, *Acta Crystallogr., Sect. A: Found. Crystallogr.* **31**, 756 (1975).
67. J.C. Woicik, C.K. Xie, B.O. Wells, *J. Appl. Phys.* **109**, 083519 (2011).
68. J.M. Rondinelli, S. Coh, *Phys. Rev. Lett.* **106**, 235502 (2011).
69. J.F. Scott, *Adv. Mater.* **22**, 2106 (2010).
70. R.J. Zeches, M.D. Rossell, J.X. Zhang, A.J. Hatt, Q. He, C.H. Yang, A. Kumar, C.H. Wang, A. Melville, C. Adamo, G. Sheng, Y.H. Chu, J.F. Ihlefeld, R. Erni, C. Ederer, V. Gopalan, L.Q. Chen, D.G. Schlom, N.A. Spaldin, L.W. Martin, R. Ramesh, *Science* **326**, 977 (2009).
71. H. Bea, B. Ziegler, M. Bibes, A. Barthelemy, P. Parush, *J. Phys. Condens. Matter* **23**, 142201 (2011).
72. A. Malashevich, D. Vanderbilt, *Phys. Rev. B* **80**, 224407 (2009).
73. J.H. Lee, K.M. Rabe, *Phys. Rev. Lett.* **104**, 207204 (2010).
74. S. Bhattacharjee, E. Bousquet, P. Ghosez, *Phys. Rev. Lett.* **102**, 117602 (2009).
75. C.J. Eklund, C.J. Fennie, K.M. Rabe, *Phys. Rev. B* **79**, 220101(R) (2009).
76. A.T. Zayak, X. Huang, J.B. Neaton, K.M. Rabe, *Phys. Rev. B* **74**, 094104 (2006).
77. A.T. Zayak, X. Huang, J.B. Neaton, K.M. Rabe, *Phys. Rev. B* **77**, 214410 (2008).
78. A.Y. Borisevich, H.J. Chang, M. Huijben, M.P. Oxley, S. Okamoto, M.K. Niranjan, J.D. Burton, E.Y. Tsymbal, Y.H. Chu, P. Yu, R. Ramesh, S.V. Kalinin, S.J. Pennycook, *Phys. Rev. Lett.* **105**, 087204 (2010).
79. J.M. Rondinelli, N.A. Spaldin, *Phys. Rev. B* **82**, 113402 (2010).
80. J. He, A. Borisevich, S.V. Kalinin, S.J. Pennycook, S.T. Pantelides, *Phys. Rev. Lett.* **105**, 227203 (2010).
81. V.K. Vlasko-Vlasov, Y.K. Lin, D.J. Miller, U. Welp, G.W. Crabtree, V.I. Nikitenko, *Phys. Rev. Lett.* **84**, 2239 (2000).
82. D.L. Proffit, H.W. Jang, S. Lee, C.T. Nelson, X.Q. Pan, M.S. Rzchowski, C.B. Eom, *Appl. Phys. Lett.* **93**, 111912 (2008).
83. S.H. Chang, Y.J. Chang, S.Y. Jang, D.W. Jeong, C.U. Jung, Y.-J. Kim, J.-S. Chung, T.W. Noh, *Phys. Rev. B* **84**, 104101 (2011).
84. Y. Segal, K.F. Garrity, C.A.F. Vaz, J.D. Hoffman, F.J. Walker, S. Ismail-Beigi, C.H. Ahn, *Phys. Rev. Lett.* **107**, 105501 (2011).
85. J. Hoppler, J. Stahn, H. Bouyanfif, V.K. Malik, B.D. Patterson, P.R. Willmott, G. Cristiani, H.U. Habermeier, C. Bernhard, *Phys. Rev. B* **78**, 134111 (2008).
86. S.J. May, C.R. Smith, J.-W. Kim, E. Karapetrova, A. Bhattacharya, P.J. Ryan, *Phys. Rev. B* **83**, 153411 (2011).
87. J.M. Rondinelli, N.A. Spaldin, *Phys. Rev. B* **81**, 085109 (2010).
88. A. Blanca-Romero, R. Pentcheva, *Phys. Rev. B* **84**, 195450 (2011).
89. N.A. Benedek, C.J. Fennie, *Phys. Rev. Lett.* **106**, 107204 (2011).
90. R. Dingle, H.L. Stormer, A.C. Gossard, W. Wiegmann, *Appl. Phys. Lett.* **33**, 665 (1978).
91. Y. Kozuka, M. Kim, H. Ohta, Y. Hikita, C. Bell, H.Y. Hwang, *Appl. Phys. Lett.* **97**, 222115 (2010).
92. T.S. Santos, B.J. Kirby, S. Kumar, S.J. May, J.A. Borchers, B.B. Maranville, J. Zarestky, S.G.E. te Velthuis, J. van der Brink, A. Bhattacharya, *Phys. Rev. Lett.* **107**, 167202 (2011).
93. B. Jalan, S. Stemmer, S. Mack, S.J. Allen, *Phys. Rev. B* **82**, 081103(R) (2010).
94. H.W. Jang, D.A. Felker, C.W. Bark, Y. Wang, M.K. Niranjan, C.T. Nelson, Y. Zhang, D. Su, C.M. Folkman, S.H. Baek, S. Lee, K. Janicka, Y. Zhu, X.Q. Pan, D.D. Fong, E.Y. Tsymbal, M.S. Rzchowski, C.B. Eom, *Science* **331**, 886 (2011).
95. P. Garcia-Fernandez, J.A. Aramburu, M.T. Barriuso, M. Moreno, *J. Phys. Chem. Lett.* **1**, 647 (2010).
96. J. Mannhart, D.G. Schlom, *Science* **327**, 1607 (2010).
97. A. Stroppa, T. Fukushima, S. Picozzi, J.M. Perez-Mato, *Phys. Chem. Chem. Phys.* **13**, 12186 (2011).
98. J. Lopez-Perez, J. Iniguez, *Phys. Rev. B* **84**, 075121 (2011).
99. J.M. Rondinelli, C.J. Fennie, arXiv:1106.0049 (2011), in press *Advanced Materials* (2012).
100. V. Gopalan, D.B. Litvin, *Nat. Mater.* **10**, 376 (2011).
101. A.D. Rata, A. Herklotz, K. Nenkov, L. Schultz, K. Dorr, *Phys. Rev. Lett.* **100**, 076401 (2008).
102. C. v. Korff Schmising, A. Harpoeth, N. Zhavoronkov, Z. Ansari, C. Aku-Leh, M. Woerner, T. Elsaesser, M. Bargheer, M. Schmidbauer, I. Vrejoiu, D. Hesse, M. Alexe, *Phys. Rev. B* **78**, 060404(R) (2008).
103. M. Rini, R. Tobey, N. Dean, J. Itatani, Y. Tomioka, Y. Tokura, R.W. Schoenlein, A. Cavalleri, *Nature* **449**, 72 (2007).
104. D. Fausti, R.I. Tobey, N. Dean, S. Kaiser, A. Dienst, M.C. Hoffmann, S. Pyon, T. Takayama, H. Takagi, A. Cavalleri, *Science* **331**, 189 (2011). □

James M. Rondinelli is an assistant professor at Drexel University in the Materials Science and Engineering Department. He received his PhD degree in materials science from the University of California–Santa Barbara (2010) under the supervision of Nicola Spaldin, followed by the Joseph Katz Distinguished Postdoctoral Fellowship at Argonne National Laboratory (2011). Rondinelli's main research interests are in the first-principles design and understanding of complex oxide- and fluoride-based materials for sustainable energy technologies and next-generation low-power electronic devices. Rondinelli can be reached by phone at 215-571-3671 and email jrondinelli@coe.drexel.edu.

Steven J. May is an assistant professor at Drexel University in the Materials Science and Engineering Department. He received his PhD degree in the field of materials science and engineering from Northwestern University in 2007. He was a postdoctoral researcher at Argonne National Laboratory from 2007 to 2009 in the Magnetic Thin Films group within the Materials Science Division. At Drexel, May's research is focused on the synthesis and characterization of complex oxide heterostructures for electronics and energy generation. May can be reached by phone at 215-571-3650 and email smay@coe.drexel.edu.

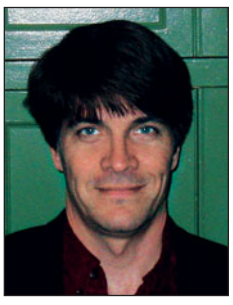

John W. Freeland is a staff scientist at Argonne National Laboratory. He received his PhD degree in condensed matter physics from Johns Hopkins University in 1996. From 1996 until 1998, he was a National Research Council Fellow at the Naval Research Laboratory. At Argonne, his research has focused on harnessing advanced probes to study surface and interface phenomena in complex oxide heterostructures. Freeland can be reached by phone at 630-252-9614 and email freeland@anl.gov.